International Journal of Control and Automation
Vol.9, No.3 (2016), pp.1-14
http://dx.doi.org/10.14257/ijca.2016.9.3.01

Analysis of the Different Topologies of Loose Coupled Rotating Transformer in Contactless Excitation System

Wang Xundong, Yu Yong, Zhang Lixin and Sui Xin

College of Electrical & Electronic Engineering, Harbin University of Science &Technology, Harbin 150080, China
wxd6158@163.com, eroserin@163.com, 15946004843@163.com, suixinsx1209@yahoo.com

Abstract

There are air gap and machining difficulty for loose coupled rotating transformer in contactless excitation system (CES). The coupling coefficient is relatively small compare with traditional transformer at the same time. There are several problems in the CES, such as loose coupled rotating transformer works inside the motor with high speed, difficult way to control, primary side and secondary side of loose coupled rotating transformer fix on the motor stator and rotor. In view of the adjacent windings type and coaxial windings type, the topology, simulation and experimental research are given in this paper. Through Ansoft 2D model identified two kinds of topology optimal working air gap is 1 mm. Verify the adjacent windings type topology of magnetic line of force closure degree is better than coaxial windings type. The simulation of Ansoft 3D model with adjacent type verifies the magnetic induction intensity is better than coaxial windings type. The experimental prototype of adjacent optimal type on CES to test the design has good transmission effect. The experimental results verify the rationality of the design of the adjacent windings type topology and accuracy, play a key role in improve the contactless excitation system in the future.

Keywords*: inductive coupled power transfer (ICPT), contactless excitation system (CES), loose coupled rotating transformer, winding topology*

Introduction

Due to the existence of electric brush and slip ring in traditional excited motor, it increases the contact resistance. Along with the increase of excitation current, electric brush and slip ring are often caused by poor contact fever. Seriously, it produces fire with burning electric brush and slip ring. The quality of electric brush affects the operation stability directly, as the same time with high failure rate[1-3]. In this paper, analyzes theory for the contactless energy transmission and puts forward design which is a brand new way of excitation called contactless excitation system (CES) that proposes to instead the traditional excitation. It uses high frequency power supply witch has loosely coupled rotary transformer as the core. On this basis, this paper emphasizes on loose coupled rotating transformer is studied in the system. The loose coupled rotating transformer is different from the relatively static transformer in the inductive coupled power transfer (ICPT). Loose coupled rotating transformer the performance of the power transmission is the core technology of this method in the contactless excitation system. It is necessary that the whole system and operation security are due to the good operation[4-7]. Literature [8] has the optimal design of magnetic circuit model transformer for ICPT. It analyzes the different winding peach sticks on the effects of overall performance. Literature [9] analyzes the adjacent windings and coaxial windings magnetic circuit model and the corresponding experimental data is presented. Literature [10] introduces the advantage of

ISSN: 2005-4297 IJCA

the S/SP compensation strategy used in ICPT system, with the voltage gain and T equivalent circuit are given at the same time. Due to the particularity of magnetic field is established, it uses the Ansoft to determine the optimal way of winding. Under 2D simulation modesl, this paper analyzes different working air gap adjacent windings topology and coaxial windings topological distribution of magnetic field lines and determines the scope of working air gap and further to determine the optimal working parameters of the air gap value. Under the 3D simulation models, this paper analyzes adjacent windings topology and coaxial windings topology of magnetic field and magnetic induction intensity parameter at the same condition. Integrated various simulation results determine adjacent windings topology under the condition of high-speed rotation, as used in the CES optimum winding of loose coupled rotating transformer topology. In combination with series-series resonance compensation strategy, the optimal air gap is 1 mm, under the conditions of the rotating speed is 3000 rpm, the experiments on transmission performance for the contactless excitation system is given.[11-13] Experimental results verified the adjacent windings topology is validity and feasibility of contactless excitation system. To further improve the contactless excitation system this new concept and key technology play a crucial role at the same time[14-16].

1. Contactless Excitation System

1.1. High Frequency Switching Power Supply in the Contactless Excitation System

The CES is designed on the basis of ICPT. It compared with traditional ICPT system the biggest characteristics are a loose coupled transformer is rotating at high speed and strict working space size. The transformer in the ICPT system is relatively static energy transmission system. A large number of literature at home and abroad show that the rotating transformer is applied to the motor magnetic force is a new field. The CES comprise DC-AC convertor, loose coupled rotating transformer, AC-DC convertor and exciting windings. The switching power supply of the CES adopted isolation type DC-DC converter. Its core is loose coupled rotating transformer with the function of isolation. The transformer can be used to replace the excitation system of collector ring and brush, realize the real meaning of brushless excitation. The CES brushless excitation system is shown in Figure 1. The whole CES is a high frequency switch power supply with special transformer. Inverter controlled switch tube by high frequency signal. At the same time, DC power supply is transformed into high frequency alternating current which is loaded into the transformer primary coil. Secondary induction of the transformer induced the high-frequency voltage, getting through a rectification filtering supply exciting windings. The secondary windings and iron core of transformer are coaxial arrangement with motor rotor. As a result of loose coupled rotating transformer, when secondary core rotating with the rotor, the magnetic circuit is almost not influenced by any factor. CES eliminate slip ring and electric brush that repeatedly wear caused by the defect completely.

1.2 Assembly of Loose Coupled Rotating Transformer

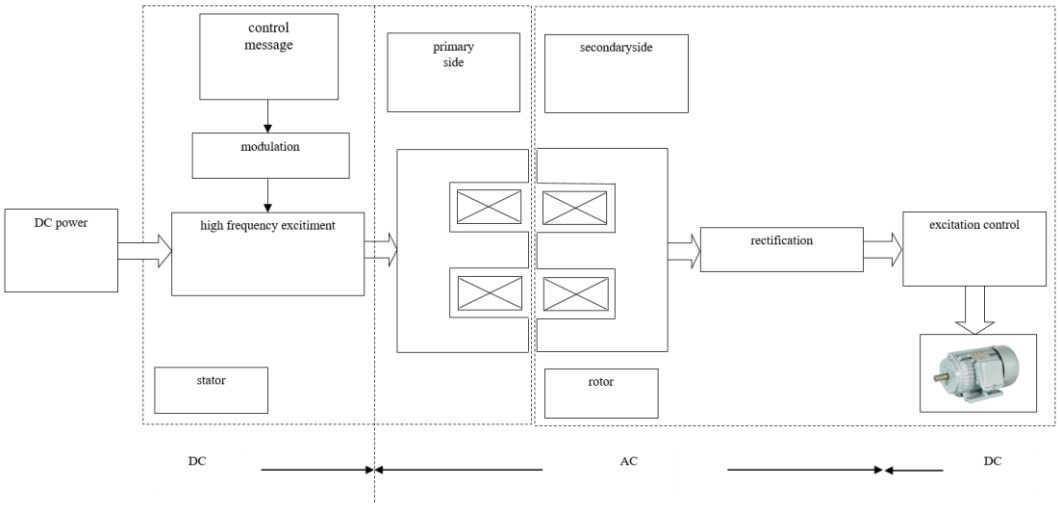

Figure 1. Contactless Excitation System

Secondary core of loose coupled rotating transformer, rectifier, motor rotor core and exciting winding are coaxial. Primary side of the Loose coupled transformer setup on the motor stator. Controller and inverter are placed in the stator shell cavity. Common DC bus is arranged on the stator casing surface. The primary core and secondary core of the loose coupled rotating transformer are relative arrangement. The primary core and secondary core of the loose coupled rotating transformer are designed between 0.5mm to 3mm. Assembly of loose coupled rotating transformer is shown in Figure 2.

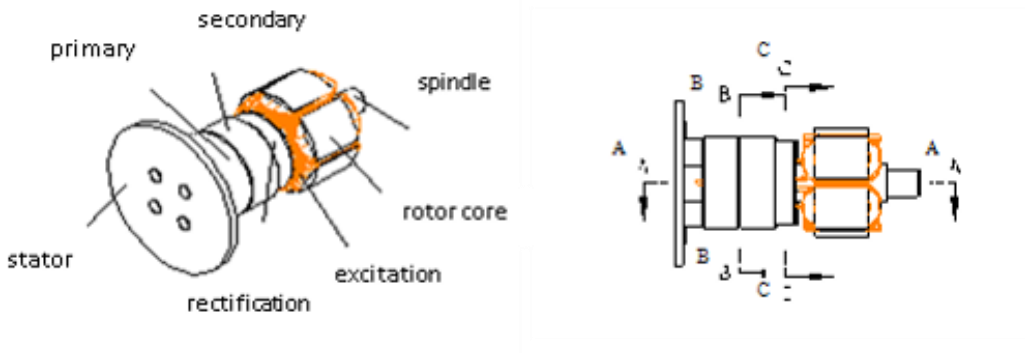

Figure 2. Assembly Drawing of the Contactless Excitation System

2. Loose Coupled Rotating Transformer Winding

In the loose coupled rotating transformer it designs two kinds of way for the winding, which called adjacent windings and coaxial windings. Both of them adopt magnetic tank ferrite as magnetic conduction path. The rotation of the magnetic tank itself can`t influence the cross section area of the magnetic and magnetic path length, as the same time requires the upper tank and the under tank under the magnetic properties and electrical properties to remain consistent. Adjacent windings topology have excellent mechanical stability and simple way of winding in other way coaxial windings have more magnetic circuit coupled area between primary windings and secondary windings. Two types of winding are loose coupled topology, whose magnetizing inductance mainly depends on the cross-sectional area of the air gap length and winding, as the same time the

leakage inductance depends on the relative position of winding. Due to the physical separation between the windings, the loose coupled rotating transformer exhibits a low-coupling coefficient. This results in storing a portion of the total supplied energy into the transformer structure itself (mainly within the air gap) rather than transferring it to the secondary. The magnetizing inductance of such a transformer is much lower than that of a conventional transformer. As a result, in addition to reflected load current, the primary winding carries an increased magnetizing current, aggravating the primary-side conduction losses.

2.1 Adjacent Windings

It can get accurate magnetic resistance model and electrical model from the physical layout of winding topology first. Adjacent windings are shown in Figure 3. The physical model of winding topology structure of adjacent is shown in 3(a). The primary windings and secondary windings are dense winding in the magnetic tank. The black part shows the air gap. Primary windings and secondary windings are putted in the two "凵" glyphs, which are nylon for insulation and two parts for stability. It is necessary to let the air gap part in good mechanical performance as far as possible under the premise of reducing the air gap, winding relative cross-sectional area to big as far as possible which causes the magnetizing inductance is increased. In order to reduce the leakage inductance value, it requires windings close winding on the magnetic tank center column. By physical model can be derived flux path model is shown in Figure 3(b).

According to the formula：

$$L = N^2 P = N^2 \frac{1}{R} \tag{1}$$

At the same time based on dual method can derive the equivalent circuit model is shown in figure 3(c). Dual physical quantities are resistance and magnetic resistance, current and magnetic flux.

2.2 Coaxial Windings

Coaxial windings magnetic resistance model is shown in Figure 4. The coaxial windings physical structure is shown in Figure 4(a). The black part shows the air gap. The winding part is putted in the function of "凵" glyph nylon skeleton internal and external inlaid. So winding has longitudinal coupling magnetic circuit. Due to the primary windings side and secondary windings side winding within a skeleton "凵" type, which is not very stable. Because of coaxial windings leads to the primary side must stick close magnetic pot at the center of the magnetic column, secondary windings as far as possible close to the center under the mechanical properties. Magnetic flux path can be concluded by physical model, which is shown in Figure 4(b). R_1-R_8 are for the flux path magnetic resistance. R_{air1} and R_{air2} are for the air gap path magnetic resistance. R_{lk}、R_{i1} and R_{i1} are for the coil magnetic resistance. Equivalent circuit is shown in Figure 4(c).

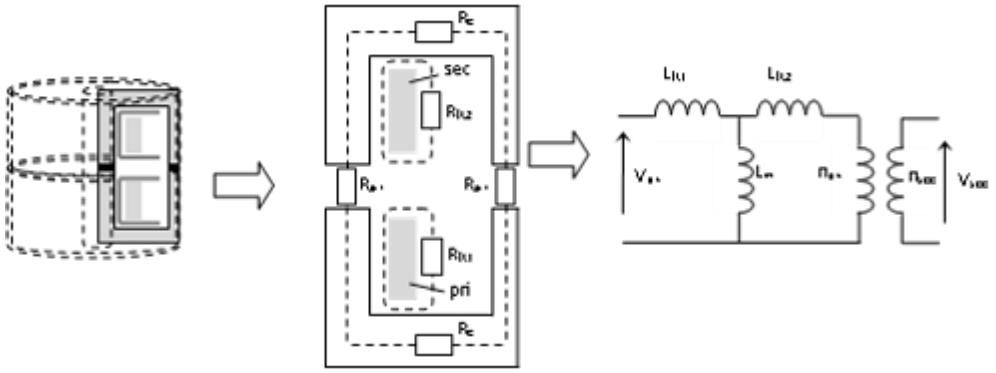

3(a) physical model 3(b) flux path model 3(c) equivalent circuit model

Figure 3. Adjacent Windings Topology Model

In loose coupled rotating transformer each part of the magnetic tank represents a part of inductance. The loose coupled rotating transformer magnetizing inductance and leakage inductance can be deduced by the following formula:

$$L_m = N_p^2 (\frac{l_c}{\mu_0 \mu_c A_c} + \frac{l_g}{\mu_0 \mu_{air} A_g})^{-1} \quad (2)$$

$$l_{lk} = N_p^2 (\frac{l_{sp}}{\mu_0 \mu_{sp} A_{sp}})^{-1} \quad (3)$$

Where N_p is the number of the primary windings. l_c is the length of the magnetic circuit. l_g is the length of air gap. A_c is the coss-sectional area. A_g is the air gap cross-sectional area. l_{sp} is the length of the equivalent magnetic circuit. A_{sp} is the equivalent sectional area.

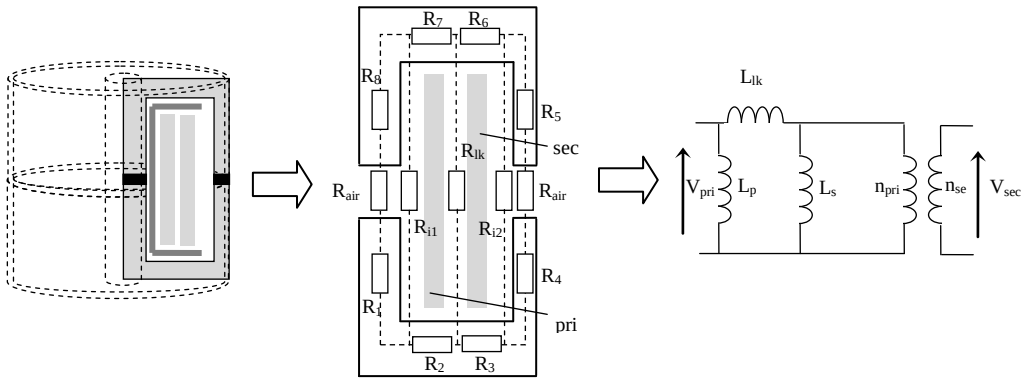

4(a) physical model 4(b) flux path model 4(c) equivalent circuit model

Figure 4. Coaxial Windings Topology Model

2.3 Compensation Strategy

For traditional transformer, the coupling coefficient is usually above 0.9, close to 1. The transformer in CES belongs to loose coupling system, which the coupling coefficient is below 0.9, some is even lower than 0.1， the more leakage inductance,

core work in the magnetization curve linear part ,due to the air gap. According to the literature above it can get the mapping the impedance:

$$Z_r = -\frac{j\omega M \dot{I}_s}{\dot{I}_p} = R_r + jX_r \tag{4}$$

Where M is mutual inductance between primary side and secondary side. R_r is mapping resistance. X_r is mapping reactance. L_s is secondary inductance. L_p is primary inductance. R_L is load resistance. When secondary side uses the series resonance compensation, the circuit is in a state of resonance.

$$\omega = \frac{1}{\sqrt{L_S C_S}} \tag{5}$$

Reflecting impedance can be simplified to:

$$Z_r = \frac{\omega^2 M^2}{Z_S} \tag{6}$$

Four different harmonic compensation strategies are obtained from series compensation and shunt compensation. In the CES, it determines the working frequency of the system, and then calculates the compensation capacitor vice edge. According to the resonant formula (5), we can get the capacitor in series compensation:

$$C_S = \frac{1}{\omega_0^2 L_S} \tag{7}$$

Where ω_0 is the frequency for secondary side resonance. Secondary side parallel resonant compensation capacitor:

$$C_S = \frac{R_L^2 \pm \sqrt{R_L^2 - 4L_S^2 L_L^2 \omega^2}}{2L_S R_L^2 \omega^2} \tag{8}$$

By (8) can clearly see that, as the load capacitance value size into nonlinear change that is not fit for CES. Series compensation is superior to the parallel compensation for the secondary side in CES. At the same time mapping impedance is described by Zr. Put (6) into (7) and (8), when secondary side uses the series compensation:

$$\mathrm{Re}Z_r = \frac{\omega^4 C_S^2 M^2 R_L}{(\omega^2 C_S L_S - 1)^2 + \omega^2 C_S^2 R_L^2} \tag{9}$$

$$\mathrm{lm}Z_r = \frac{-\omega^3 C_S M^2 (\omega^2 C_S L_S - 1)}{(\omega^2 C_S L_S - 1)^2 + \omega^2 C_S^2 R_L^2} \tag{10}$$

When secondary side uses the shunt compensation:

$$\mathrm{Re}\, Z_r = \frac{\omega^4 M^2 R_L}{R^2 (\omega^2 C_S L_S - 1)^2 + \omega^2 L_S^2} \tag{11}$$

$$\mathrm{lm}Z_r = \frac{-\omega^3 M^2 [C_S R_L^2 (\omega^2 C_S L_S - 1) + L_S]}{R_L^2 (\omega^2 C_S L_S - 1)^2 + \omega^2 L_L^2} \tag{12}$$

Re is real part. Im is imaginary part. Set the equivalent total impedance of primary Z_t, when the primary side with series compensation:

$$Z_t = j\omega L_p + \frac{1}{j\omega C_p} + Z_r \quad (13)$$

When primary side the parallel compensation:

$$Z_S = \frac{1}{j\omega C_p + 1/j\omega L_p + Z_r} \quad (14)$$

The real part of Z_t is the active power. The imaginary part of Z_t is the reactive power. When $\omega = \omega_0$, the calculation results can be expressed as shown in Table 1.

From formula (7) and the expression in Table 1, capacitance and inductance are in the resonance. Its expression is very simple, at the same time reaction reactance is 0.There are higher output current and output power when it is in the series-series compensation strategy at *f*=100kHz.

3. Simulation and Experimental Analysis

3.1 2D Simulation Results and Analysis

According to the adjacent windings topology and coaxial windings topology Ansoft 2D models are established respectively. The simulation of the magnetic field lines at 1mm and 3mm air gap is shown in Figure 5. The 2D simulation parameters are as follows: driving frequency f=100kHz,speed is 3000 rpm.

Table 1. Expressions of Primary Side Capacitance

resonant topology	primary capacitance
SS	$C_P = \frac{1}{\omega_o^2 L_P}$
SP	$C_P = \frac{1}{\omega_o^2 (L_P - M^2/L_S)}$
PP	$C_P = \frac{L_P - M^2/L_S}{(M^2 R_L/L_S^2)^2 + \omega_o^2 (L_P - M^2/L_S)^2}$
PS	$C_P = \frac{L_P}{(\omega_0^2 M^2/L_S^2)^2 + \omega_o^2 L_P^2}$

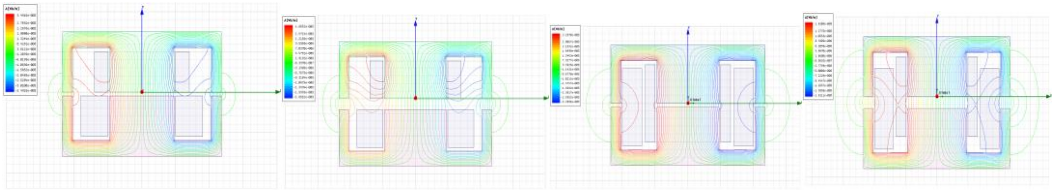

(a) 1mm adjacent windings | (b) 3mm adjacent windings | (c) 1mm coaxial windings | (d) 3mm coaxial windings

Figure 5. Abuts and Nested Type Topology Model Graphs of Magnetic Force Simulation Diagram

According to the simulation diagram 5(a) and 5(b) ,it can be clearly seen that adjacent windings topology, when working at 1mm air gap loose coupled rotating transformer can establish good closed magnetic field lines, it can reach 3.5-005 Wb/m. When working at 3mm air gap, lines of magnetic force divergence degree is higher, it can only reach

1.8-005 Wb/m. A large part of magnetic field lines were closed through the air gap, leading the decrease of overall transmission performance of loose coupled rotating transformer inevitably. By Figure 5(c) and Figure 5(d) we can get the same conclusion. In the coaxial windings topology 1mm magnetic field lines were closed in a good degree. By contrast the distribution of 3mm magnetic field lines, under the premise to meet the mechanical properties of high speed, no matter which topology we can obtain that 1mm is the optimal working air gap.

3.2 3D Simulation Results and Analysis

According to the adjacent windings topology and coaxial windings topology Ansoft 3D models were established respectively. Adjacent windings 3D simulation model and coaxial windings 3D simulation model are shown in Figure 6. The dark part of the adjacent windings 3D simulation model are the primary side windings and secondary side windings, the translucent portion is tank. The dark part of the coaxial windings 3D simulation model is the secondary side windings, the translucent portion is tank and primary side windings.The subdivision graph of adjacent windings and coaxial windings are shown in Figure 7 and Figure 8. 3D simulation parameters are shown in Table 2.We can obtain that simulation waveform at any time through simulation, the simulation figure of adjacent windings at 1e-005s, 2e-005s, 0.0005s and 0.001s is shown in Figure 9. The simulation figure of coaxial windings at 0.0005s and 0.001s is shown in Figure 10.

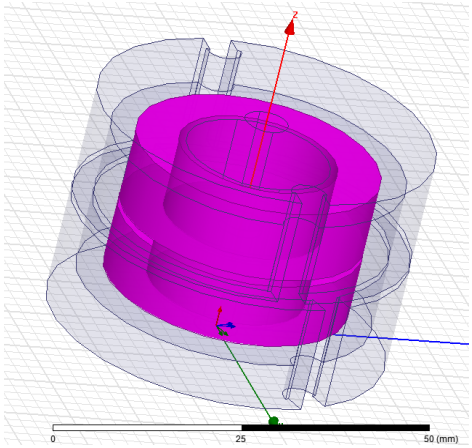

(a) Adjacent windings 3D simulation model

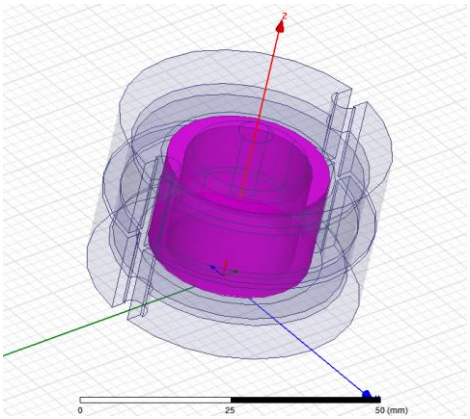

(b) Coaxial windings 3D simulation model

Figure 6. Adjacent Windings 3D Simulation Model and Coaxial Windings 3D Simulation Model

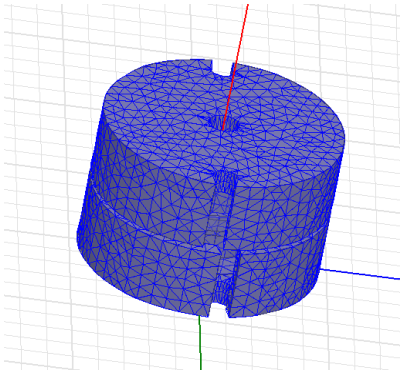

(A) Triangulated Graph of Adjacent Windings Tank

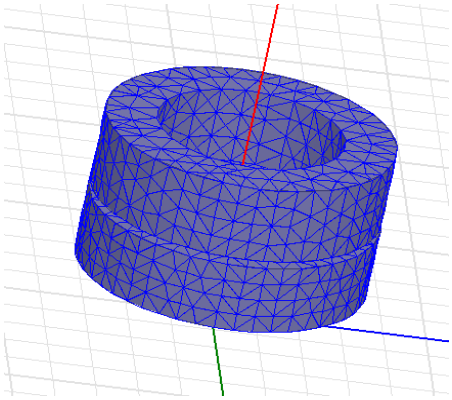

(B) Triangulated Graph of Adjacent Windings

Figure 7. Adjacent Windings 3D Triangulated Model

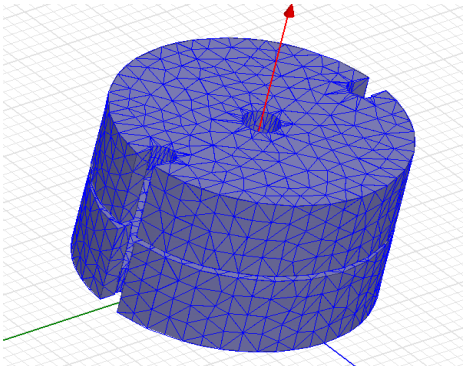

(a) Triangulated graph of adjacent windings tank

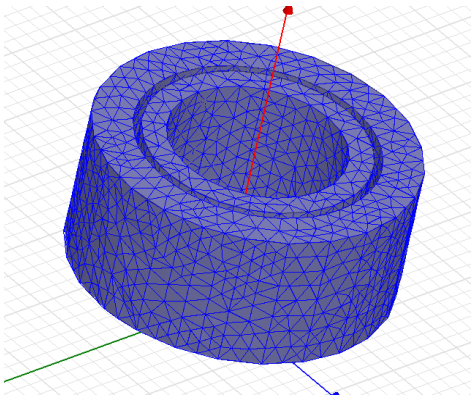

(b) Triangulated graph of coaxial windings

Figure 8. Coaxial Windings 3D Triangulated Model

Figure 9(a) and Figure 9(b) shows that the magnetic induction adjacent windings topology has established at 1e-005s and 2e-005s is relatively weak, the maximum is only 6.196e-004T and 1.174e-003T. The magnitude that magnetic induction achieved at 2e-005s and the stable magnetic induction are the same. The figure shows that the maximum of magnetic induction are 4.883e-003T and 6.779e-003T at 0.005s and 0.01s. From the above four groups of data, the magnetic induction is basically stabilized at 0.001s.

Table 2. 3D Parameters of Simulation

description	parameter
simulation time/t	0.001
simulation step/t	1e-007
motion parameter /rpm	3000
triangulated graph of windings/mm	4
triangulated graph of tank /mm	8

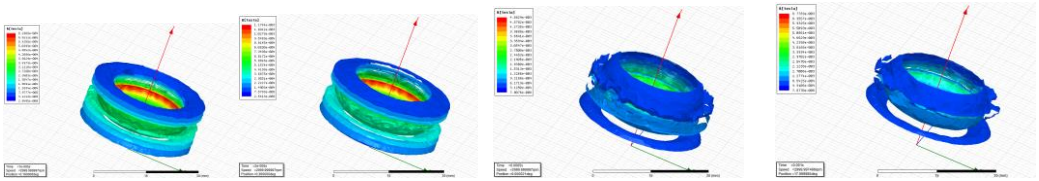

(a) 1e-005s (b) 2e-005s (c) 0.0005s (d) 0.001s

Figure 9. Adjacent Windings Type Topology Simulation Scalar on the Magnetic Induction Intensity

(a)0.0005s (b)0.001s

Figure 10. Coaxial Windings Type Topology Simulation Scalar on the Magnetic Induction Intensity

Figure 10(a) and Figure 10 (b) show that the maximum of coaxial windings topology magnetic induction are 8.883e-004T and 1.770e-003T at 0.0005s and 0.001s. Comparing with two sets of data shows that the magnetic induction is basically stabilized at 0.001s.

In connection with relatively stable magnetic intensity, at 0.0005s and 0.001s, it compare with the average of magnetic induction intensity between adjacent windings topology and coaxial windings topology. It obtains that average value of the adjacent windings magnetic induction is 2.445e-003T at 0.0005s, it is much larger than the average value of the coaxial windings magnetic induction. By analyzing the above data show in the same 1mm optimum working range, combining with the pros and cons of the mechanical properties, the magnetic field which adjacent windings topology established is better than coaxial windings topology. It obtain that adjacent windings topology is optimal in the CES.

3.3 Experimental Results and Analysis

The power input of CES is 12V and operating frequency f=100 kHz. LM5035 provides excitation energy through the primary side which is transferred to the secondary side by loose coupled rotating transformer. The power drives the excitation of the secondary side of loose coupled rotating transformer at high-speed rotation. Due to the transformer in CES is the loose coupled type, the rotating transformer exhibits a low-coupling coefficient. Therefore, it is necessary to add the compensation strategy which can obtain good transmission characteristics. Add series-series compensation network and adjacent windings, with the air gap is 1mm-3mm. Primary side voltage waveform and secondary voltage waveform are shown in Figure 11.Where up is the primary voltage and us is the secondary voltage. Type in the adjacent topology winding mode with R=1Ω and the speed of motor is 3000 rpm which has the similar strain ratio characteristics of tightly coupled. Primary side voltage is about 6V and the secondary side is about 12V. It has good transmission performance, at the same time, effectively reduces the influence of the leakage inductance. With the increase of voltage in the secondary side it can obtain more transmission power.

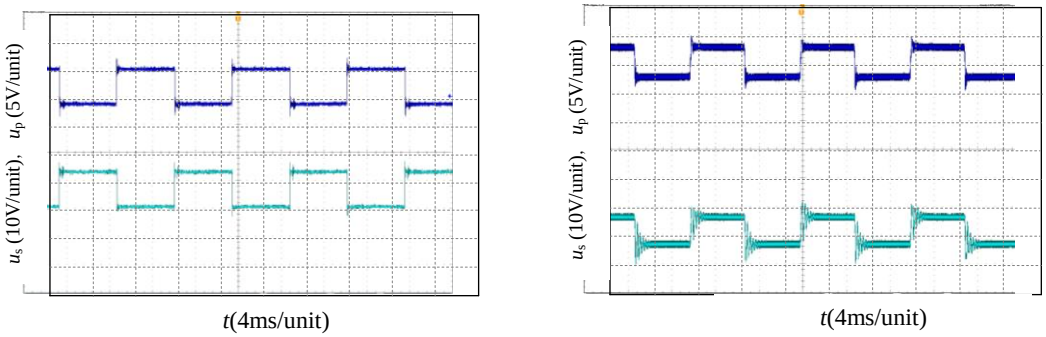

(a) air gap is 1mm (b) air gap is 3mm

Figure 11. Load 1Ω□Series - Series Resonance Compensation Waveform Graph

When working air gap increases from 1mm to 3mm, it can be seen that the voltage decay is relatively obvious. At 3mm, although the adjacent windings have series-series compensation the transmission capacity is unable to meet the requirements. It is consistent with the result when optimal gap is 1mm in previous section.

4. Conclusion

(1) For the loose coupled rotating transformer, when using adjacent windings and coaxial windings, Ansoft 2D models were established at different working air gap. From the relationship between the magnetic induction coupling strength and air gap, it can draw the conclusion that the optimal working range are 1mm whether the way of winding topology.

(2) Contrast Ansoft 2D and Ansoft 3D simulation, it is easy to see in the optimal working air gap is 1mm. In the same working conditions for different winding topology that the magnetic field created by adjacent windings is better than coaxial windings from that several factors that density of line of magnetic force, magnetic induction intensity and the magnetic field settling time. Adjacent windings are the optimal for the bran-new CES itself.

(3) The experimental results show that in the adjacent windings topologies with series-series compensation strategy that loose coupled rotating transformer the best work air gap is 1 mm and the adjacent windings topologies is the best way. In the case of high speed loose coupled rotating transformer has good transmission performance. This study further shows that loose coupled rotating transformer in CSE is feasibility and accuracy.

Acknowledgements

The project was supported by the Project Supported by National Natural Science Foundation of China (51177031)

References

[1] R. Raja, I. Rakib and I. Mohammad, “Real time estimation of parameters for controlling and monitoring permanent magnet synchronous motors”, IEEE International Electric Machines and Drives Conference, **(2009)**, pp. 1194-1199, Miami, United States.
[2] D. Jianning, H. Yunkai and J. Long, “Review on high speed permanent magnet machines including design and analysis technologies”, Proceedings of the CSEE, vol. 34, no. 27, **(2014)**.
[3] M. Hao and S. Xuan, “Journal of Design of voltage source inductively coupled power transfer system with series compensation on both sides of transformer”, Proceedings of the CSEE, vol. 30, no. 15, **(2010)**.
[4] K. Maki, H. Funato and L. Shao, “Motor modeling for EMC simulation by 3-D electromagnetic field analysis”, IEEE International Conference on Electric Machines and Drives Conference, **(2009)**, pp. 103-108, Miami, United States.
[5] C. Martis, H. Hedesiu and B.Tataranu, “High-frequency model and conductive interferences of a small doubly salient permanent magnet machine”, IEEE International Conference on Industrial Technology, **(2004)**, pp. 1378-1383, Hammarnet, Tunisia
[6] G.A. Covic, J.T. Boys and A.M.W. Tam, “Self tuning pick-ups for inductive power transfer”, IEEE Power Electronics Specialists Conference, **(2008)**, pp. 3489-3494, Rhodes, Greece.
[7] J.Y. Lee and H.Y. Shen, “Contactless inductive charging system with hysteresis loop control for small-sized household electrical appliances”, 27th IEEE Applied Power Electronics Conference and Exposition, **(2012)**, pp. 2172-2178, Orlando.
[8] H. Ying, C. Ence and T. Houjun, “Journal of Application of model fellow control on contactless inductive power transfer”, Journal of Harbin University of Science and Technology, vol. 18, no. 1, **(2013)**.
[9] J.P.C.S. meets, D.C.J. Krop, J.W. Jansen, M.A.M. Hendrix and E.A. Lomonova, “Optimal Design of a Pot Core Rotating Transformer”, Energy Conversion Congress and Exposition, ECCE, **(2010)**, pp. 4390-4397.
[10] H. Jia, C. Qianhong and Y. Kaiqin, “Journal of Analysis and Control of S/SP Compensation Contactless Resonant Converters”, Proceedings of the CSEE, vol. 33, no. 33, **(2013).**
[11] V. Ruuskanen, M. Niemela and J. Pyrhonen, “Journal of Modeling the brushless excitation system for a synchronous machine”, IET Electric Power Applications, vol. 3, no. 3, **(2009).**
[12] K.D. Papastergiou, “Journal of An Airbone Radar Power Supply With Contactless Transfer of Energy-Part I: Rotating Transformer”, IEEE Transactions on industrial electronics, Selleschy, vol. 54, no. 5, **(2007)**.
[13] K.D. Papastergiou and D.E. macpherson, “Contact-less Transfer of Energy by means of a Rotating

Transformer", IEEE ISIE, **(2005)**, pp. 1735-1740, Dubrovnik, Croatia.
[14] A.J. Moradewic and M.P. Kazmierkowski, "Journal of Contactless Energy Transfer System With FPGA-Controlled Resonant Converter", IEEE Transactions on industrial electronics, vol. 57, no. 9, **(2010)**.
[15] Y. meicun, W. Xudong, L. Jinfeng and Y. Yong, "Journal of Analysis of contactless excitation power supply resonance compensation. Electric Machine and Control", vol. 19, no.3, **(2015)**.
[16] C. Baoyuan, Z. Lishuang and W. Xi, "Journal of Study on single-phase inverter controller based on H_∞control algorithm", Journal of Harbin University of Science and Technology, vol. 15, no. 4, (**2010)**.

